



A Novel Medical Image Segmentation Using Neutrosophic Sets With Slope Variation

Sangeeta K Siri¹, S Pramod Kumar², Mrityunjaya V. Latte³

¹Global Academy of Technology, Bengaluru, Karnataka, India, sangeetamk28@gmail.com

²Jawaharlal Nehru National College of Engineering, Shivamogga, India.

³East Point College of Engineering, Bengaluru, Karnataka, India.

Abstract: Computer-Aided Diagnostic methods demand the precise segmentation of medical images. The important stage in diagnosis is the extraction of the Region of Interest (ROI). Illustration of the image in a more meaningful way is the aim of segmentation. Segmentation finds extensive use in computer vision, object recognition, image recovery based on the content, etc. In the proposed model, Slope Variation Scatter (SVS) plot of image is obtained to compute vertices of Neutrosophic Gaussian Function (NGF). The SVS describes global variation rate of image histogram. In this, the crests represent local mean of pixels/ certainty mean and valleys represents uncertainty mean. A novel NGF is membership function designed to convert abdominal Computed Tomography (CT) to Neutrosophic Subsets (NS). The NS comprises of object, nonobject and edge subsets. The Object Subset (OS) represents liver or kidney, Nonobject Subset (NOS) represents background of liver/kidney and Edge Subset (ES) represents edges of liver or kidney. The proposed model is experimented on 106 abdominal CT images to segment the liver and kidney accurately. The experimental outcomes are compared with Fuzzy C Means algorithm (FCM), show that the anticipated framework is proficient of segmenting an intended organ automatically and precisely. The proposed model achieves average accuracy, Relative Volume Difference (RVD) and Dice Similarity Factor (DSF) for liver are 91.01%, 8.23% and 89.61% respectively. The average accuracy, RVD and DSF for kidney are 91.11%, 5.96% and 91.45% respectively.

Keywords: Neutrosophic Set, Slope Variation Scatter plot, Segmentation, Neutrosophic Gaussian Function, Computed Tomography, liver segmentation, kidney segmentation.

1. Introduction

An essential stage in image processing is image segmentation, which separates an image into distinct areas having similar attributes such as colour, texture, pixel intensity, edges, etc and confiscates objects of interest that usually is called Region of Interest (ROI) [1, 2]. As a result, the process of image segmentation is adopted to fix the boundaries to objects. It results in each pixel in an image being given a unique label [2]. The image is renewed into identifiable data structure through image segmentation. It also targets feature extraction and

parameter measurement, which simplifies advance image analysis. The advance image analysis is essential in the many more fields like military [8], remote sensing [6], industrial automation [9], transportation [3, 4], medicine [5], communication [7], military [8], etc.

In medical field, segmentation has grabbed lot of attention since they are used in treatment planning, lesion location, anatomical structural research, estimating disease likelihood, disease diagnosis, surgery planning, carry out virtual surgical simulations, organ development study, functional mapping, clinical measurement [14], etc. Image segmentation reduces redundant information and facilitates object visibility [10]. The image analysis is straightway impacted by superiority of image segmentation [11]. To diagnose and to choose appropriate therapy, image segmentation has proven to be one of the most useful technologies available to medical practitioners. It is anticipated that adaptive algorithms will support and ease the process of making medical decisions.

In the last forty years, various image segmentation algorithms/models were designed. But still the topic is open for obtaining a single segmentation algorithm/ model which can be applied on all types of images to achieve accurate segmentation. It is sometimes hard to predict which segmentation algorithm is better for a specific object segmentation. This is due to different imaging characteristics, variances in the patients under consideration, small differences in the task being addressed, and variations in the validation metric [12]. Medical segmentation is the complex field in image processing because variations in light and distance are two irregular circumstances that might be present in medical images while acquiring the image. Additionally, the resolution of the images may be low, which complicate the identification of minor lesions [11]. Medical images may also include hair, reflections, and shadows, all of which might make it difficult to distinguish and analyze lesions. In addition, in medical images, variations in brightness, illumination, movement of patient in capturing the images, etc. make image unclear. Also, biomedical images may be blurry because of inheritance characteristic of image acquisition device and due to movement of patient, which affect the quality of image [13]. Since biomedical images are fuzzy, edges are not crispy, tissues are soft and have the same pixel intensity, etc. make the segmentation process very complex. Because of these issues and variations in tissue distribution among the human population, segmentation findings need to be interpreted with some degree of ambiguity. As a result, medical image segmentation can be thought of as an unsolved problem.

The automatic segmentation techniques can be classified as supervised and unsupervised. Supervised techniques are one which require the contribution of an operator throughout the process of segmentation while unsupervised techniques usually operator contribution only after accomplishment of segmentation process. Unsupervised techniques are desired to produce replicable outcomes. Whilst operator contribution is still necessary for error rectification in the incident of an unsatisfactory outcome.

A Fuzzy Set (FS) defines only two values, “true” and “false” which is sometime difficult to handle real life difficulties [16]. The extension/generalized form of Intuitionistic Fuzzy Set is Neutrosophic Set (NS) which is a burgeoning tool to handle real life problems like human thoughts [16], medical image analysis [15], etc. The NS deals with ambiguity, inconsistency, and uncertainty for computation and decision making. The NS consists of three membership function named as Object Subset (OS) or true subset, nonobject subset (NOS) or false subset and indeterminacy subset or Edge Subset (ES) which are independent entities. For all real-life decision-making problems, NS is more flexible and efficient since it assigns the same weight to the indeterminacy subset as it does to OS and NOS. NS is also versatile because in addition truth components, it can accommodate indeterminacy and false components, whereas FS cannot handle with all these. Because of all these reasons, NS has many practical applications in various fields like image processing, decision making, data mining, block chain, marketing, medicine, strategic planning, etc [17].

Transforming the image pixel values into NS using neutrosophic functions or membership functions (MFs) is called as neutrophication process, predominantly considering indeterminacy values that result from nebulosity. It has become customary to confine the MFs to well-known formats such as sigmoid, standard Gaussian, trapezoidal, and triangle forms [17]. Developing MFs is a crucial effort for Neutrophication process as the MFs determine the success of an approach. The method in which ambiguity and vagueness are handled in software metrics is aided by the theory of neutrosophic system. Using MFs in an expert system inside a neutrosophic environment definitely answer the problem's uncertainty. Commonly used MFs in real time are S/Z-shaped, trapezoid, triangle, gauss, and bell-shaped. Choosing proper MF for specific application is tricky and deciding factor for success of neutrophication process. Neutrosophic Gaussian Function (NGF) provides low computational complexity. For this reason, a novel NGF is designed to convert CT images to its NS domain. The NGF parameters play key role in defining the MF and accuracy of transformation.

we are exploiting Slope Variation Scattering plot of image which directly describes the pixel variation rate of image histogram. The crests represent the mean/certainty level of local pixels and valleys symbolizes uncertainty mean. The valleys can be taken as thresholds to eliminate background or crests values can be taken to separate objects from the background.

Segmenting spleen, kidney, liver, etc. from abdominal CT scan is most demanding as well as complex task job in Computer Aided Diagnostics system since organs are complex in shape, organs are close to each other, have same pixel intensity level, etc. Because of these reasons many segmentation algorithms fail to segment precisely. This motivated us to propose a novel model based on SVS and NS theory which accurately segments the intended organ from abdominal CT scan automatically and precisely.

The article is organized as follows. Section 2 describes literature survey, section 3 explains proposed model, section 4 illustrates experimental results, section 5 depicts quantitative analysis and last section is about conclusions.

2. Literature Survey

Panimalar et al [18] used haar wavelet transform on NS to denoise the image. The level of indeterminacy of image is obtained using NS entropy. The proposed method is compared with commonly used denoising methods like median and wiener filter, providing better quality image. Thanikachalam V [19] et al proposed accurate NS segmentation with Optimal Deep Brief Network Model for diagnosis of Diabetic Retinopathy (DR). The DR dataset was utilized for experimentation, providing promising outcome compared to existing technique. The NS theory provides indeterminacy present in image with high efficacy. This property was utilized by Talouki AG et al [20] for image completion to fill holes and decrease intensity ambiguity in the image. The dental radiographic image was mapped to NS domain by Datta S [21] et al to acquire initial segmentation of ROI. The ROI was amended by FCM algorithm to obtain accurate outcomes. The model has been evaluated on publically available dataset with the accuracy of 93.2%. Ziyun Wang et al [22] proposed U-NET which includes expectation maximization attention mechanism to segment kidney and its tumour. This model is implemented on kits19 dataset reaching dice coefficient of 0.95 and 0.83 for kidney and tumour segmentation respectively.

Liver is one of the difficult organs to separate from the abdominal CT scan because edges are not clear. Sangeeta et al. [23] converted CT image to NS and morphological operations are utilized to detach liver image from CT scan and Fast Marching Method

(FMM) is exploited to mark edge of liver. Sangeeta et al. [24] combined advantages of NS domain of abdominal CT scan image and Chan-Vase algorithm to acquire specific liver image. Sangeeta et al. [25] proposed accurate liver segmentation algorithm using Expectation-Maximization (EM) with optimal quantity of clusters (K). The K value is accomplished by finding mean of all local peaks which delivers minimum and maximum thresholds to detach liver from CT scan using threshold-based segmentation. Statistics of pixel intensity distribution was studied to obtain threshold values to isolate liver from CT scan by Sangeeta et al [26]. The liver edges are corrected by improved chain code and Bresenham pixel interconnection approaches. This delivered an exact liver image. Wang Z [27] proposed new model based on Slope Difference Distribution (SDD) of image to find the thresholds to separate two or more objects in the image. The maximum True Positive computation for cells as 93.4%. Wang Z et al. [28] anticipated novel segmentation model based on non-iterative clustering approach. The model was applied on fuzzy image to isolate fuzzy object unerringly. Wang Z [29] et al. achieves shape features of object as sparse characteristics using SDD. In this paper, minimum distances between SDD are utilized to recognize the object. Sangeeta et al. [30] achieves accurate threshold values by SDD features of liver image. By applying these, liver image is separated from CT scans precisely. Subsequently FMM is used to put outline for liver image in CT scan image. Nayantara et al [31] proposed Deep Learning framework in combination of leaky ReLU layers and SegNet to extract intact precise liver image from CT scan dataset. This framework achieves Dice Coefficient of 96%. Zhang et al [32] anticipated a novel Deep Learning model which extracts circular regions to detect hepatic steatosis to obtain exact liver image from abdominal CT scan with 95% confidence interval. Leube et al [33] anticipated automated kidney segmentation from CT images. In this, two types of segmentation are performed initially. First segmentation is performed on CT images and is called as detail segmentation; second segmentation is performed on PET images, and it is called as coarse segmentation. Subsequently, 5 different UNET is implemented to obtain final kidney segmentation. The framework is performed on 20 different patients. Cao et al [34] designed automatic kidney segmentation network based on deep neural network. This integrates decoding module and multi-scale spatial perception module. This achieves precision of 98.52%. Prashanta et al [35] proposed modified breadth first algorithm for finding shortest path (SP) for connected networks in neutrosophic environment. In this article, neutrosophic edge length is transformed to crisp edge lengths to find SP. Rajesh et al [36] suggested a model to handle

multiple criteria and ambiguous data. To implement this, Pythagorean NS Theory is designed to provide beneficial tool for decision-making in selecting a partner. Ivan et al [37] utilized neutrosophic logic in decision making for disease prevention program and health promotion. The aim of the proposed model is to use neutrosophic logic in resource allocation effectively in ambiguous condition in the field of public health. Srinivasan S et al [38] designed combined endeavour of multidimensional Convolutional Neural Network (CNN) and UNET. This framework is implemented on dermoscopy images to segment skin lesions. The proposed model shows better performance compared to traditional UNET. Shahat et al[39] proposed combined venture of NS theory and optimization algorithms to segment brain CT images. Neutrosophication operation is performed using S membership function providing precise segmentation results. Mostafa et al [40] addressed noise and ambiguity present in medical images. The authors have designed different types of filters based on NS theory to remove noise in X-ray images.

3. Proposed Model

The proposed model is presented in two parts. In part 3(a), calculation of Slope Variation Scatter (SVS) of the object image is obtained to formulate parameters of NGF and in part 3(b), CT scan image is transformed to NS domain to acquire accurate segmentation of an object image from the source image.

3(a) Formulation of parameters of NGF from SVS of image.

The SVS was first defined in [43] by Wang Z to obtain threshold to segment the laser line. The SVS describes global variation rate of image histogram. The crests represent the local mean/ certainty mean of pixels and valleys represents uncertainty mean. The valleys can be taken as thresholds to eliminate background or crests values can be taken to separate objects from the background. The SVS of object histogram is defined as rate of variation of pixel scattering and is designed as follows.

Step 1: The abdominal CT scan image is converted to grey scale and resized to 512X512 and assumed to be having Gaussian distribution.

Step 2: Crop small part of object (may be liver/ kidney/ spleen) to find its SVS.

Step 3: Compute normalized histogram scattering $P_N(x)$ by following formula.

$$P_N(x = i) = \frac{n_i}{n_j}, i = 0 \dots \dots 255 \quad (1)$$

Where n_i represents the frequency of the pixel value i , and highest frequency that ensues at j in the interval [0 to 255] is indicated by n_j .

Step 4: A noise-removal filter based on the Discrete Fourier Transform (DFT) is utilized.

(a) The normalized histogram scattering is converted into frequency domain by the DFT as follows.

$$F(H) = \sum_{x=0}^{255} P(x) e^{-\frac{j2\pi Hx}{255}}, \quad H = 0, \dots, 255 \tag{2}$$

Where $F(H)$ ($H=0, \dots, 255$) corresponds Fourier Transformation (FT) of the normalized histogram scattering $P_N(x)$.

(b) The high frequency components from 20 to 255 are eliminated and low frequency components are retained as follows.

$$F'(H) = \begin{cases} F(H); H = 0, 1, \dots, 19 \\ F(H); H = 235, \dots, 255 \\ F(H); H = 20, 21, \dots, 234 \end{cases} \tag{3}$$

Where $F'(H)$ ($H=0, \dots, 255$) represents the filtered FT of $P(x)$ by applying Low Pass filter of bandwidth (BW) of 20. The trial-and-error analysis is performed on large CT scan dataset yielded $BW=20$.

(c) Subsequently, frequency domain of an image $F'(H)$ is converted to spatial domain by using equation (4).

$$P'_N(x) = \frac{1}{T} \sum_{H=0}^{255} F'(H) e^{\frac{j2\pi Hx}{255}} \quad x=0, \dots, 255 \tag{4}$$

$P'_N(x)$ is smoothed histogram scattering.

Step 5: Every point on $P'_N(x)$, two slopes are computed: one on the left and second on the right to compute Slope Variation (SV). The N adjacent points on each side are fitted into a line model to calculate slope values as follows.

$$y_i = ax_i + b; \quad i=1, 2, \dots, N \tag{5}$$

Where a and b are coefficients of fitted line and they are calculated by following equation.

$$[a, b]^T = (C^T C)^{-1} C^T Y \tag{6}$$

C and Y in equation (6) is obtained by following equation (7) and (8).

Where $C = \begin{bmatrix} x(1) & \dots & 1 & \dots \\ x(2) & \dots & 1 & \dots \\ \vdots & \dots & \vdots & \dots \\ x(N) & \dots & 1 & \dots \end{bmatrix}$ (7)

$$Y = [y_1, y_2, \dots, y_n]^T \tag{8}$$

where $(x_i, y_i); i = 1, 2, \dots, N$ is the coordinate of the i^{th} point on the filtered data. In this article, the value of N is chosen as 20.

Let $a_1(i)$ and $a_2(i)$ are two slopes at i^{th} point on right-hand and left-hand side respectively. The Slope Variation (SV) at i^{th} point as computed as follows.

$$SV(i) = a_2(i) - a_1(i) \dots \text{where } i = N + 1 \dots \dots \dots 255 \quad (9)$$

Here SV (i) indicates SVS of object. The crests and valleys are computed by equating the derivative of SV (i) to 0. The crests C_i where $i=1 \dots \dots \dots n_c$ and valleys V_i where $i=1 \dots \dots \dots n_v$, with largest local variation in SVS are obtained. The crests symbolize to certainty of pixels values in the object and valleys symbolize to uncertainty pixel values in the object region.

Step 6: Find pixel values which is having highest crest which corresponds to centre (*cent*) of NGF. Consider two pixel values whose crests are placed on left-hand side of *cent* named as x_1 and x_2 and two pixel values whose crests are positioned on right-hand side x_3 and x_4 . Now, ($x_1, x_2, \text{cent}, x_3, x_4$) are parameters of NGF to convert the image to the NS domain. The NGF and its parameters are described in figure 1.

3.2 NS framework:

The word “Neutrosophic” is combination of two Latin words, “neuter” means “neutral” and “sophia” means “wisdom”. This theory wisely and accurately finds indeterminacy in fuzzy images. NS theory was introduced by Smarandache F in 1999 [42,45] which is commonly used in decision making process [46] in real world problems. In recent days, NS theory is utilized in fault detection, optimum design, medical diagnosis, decision making, image processing, computational intelligence, etc. NS has wide range of applications which covers most of the areas since it deals with vagueness and indeterminacy [46]. Any image in NS theory consists of three subsets named as (i) Object Subset (OS) or true Subset (ii) Non-Object Subset (NOS) or false subset and (iii) Edge Subset (ES) or indeterminacy subset. The given image is transformed to NS domain utilizing NGF as follows.

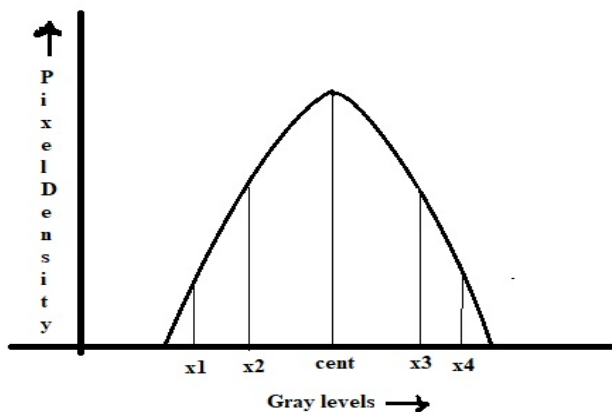


Figure 1: NGF Graph

Step 1: Compute Object Subset (OS) and Non-Object Subset (NOS) using novel SMF as follows.

$$OS(x, y) = \Pi(A_{xy}, x_1, x_2, cent, x_3, x_4) = \begin{cases} 0 & \square & A_{xy} < x_1 & \square & \square \\ \frac{(A_{xy}-x_1)^2}{(x_4-x_1)^2} & \square & x_1 \leq A_{xy} < x_2 & \square & \square \\ 1 - \frac{(A_{xy}-x_2)}{(x_4-x_2)} & \square & x_2 \leq A_{xy} < cent & \square & \square \\ 1 - \frac{A_{xy}-x_3}{(x_4-x_3)} & \square & cent \leq A_{xy} < x_3 & \square & \square \\ \frac{(A_{xy}-x_4)^2}{(x_4-x_3)^2} & \square & x_3 \leq A_{xy} < x_4 & \square & \square \\ 0 & \square & A_{xy} > x_4 & \square & \square \end{cases} \quad (10)$$

$$NOS(x, y) = 1 - OS(x, y) \quad (11)$$

OS represents the degree of being object pixels, and NOS presents the degree of background pixels.

Step 2: Edge subset is obtained as follows.

(a) Let $A(x, y)$ be pixel intensity value at (x, y) and $\hat{A}(x, y)$ represents local mean.

$$\hat{A}(x, y) = \frac{1}{T} \sum_{m=i-w/2}^{i+w/2} \sum_{n=i-w/2}^{i+w/2} A(m, n) \quad (12)$$

Where w is size of sliding window. Let $e(x, y)$ as absolute value of pixel intensity at $A(x, y)$ and its local mean $\hat{A}(x, y)$. Let e_{min} and e_{max} be lowest and highest value of $e(x, y)$ in whole object image.

(b) Then edge subset (ES) is formulated using equation (13).

$$ES(x, y) = \frac{e(x, y) - e_{min}}{e_{max} - e_{min}} \quad (13)$$

Step 3: Convert image OS, NOS and ES into binary image.

Image segmentation is characterized by homogeneousness of local region. The homogeneity characteristic of image is obtained by discontinuity of intensity corresponds to the variations in grey levels and Standard Deviation (SD) which describes dissimilarity within local region. The homogeneousness is characteristics of foreground and background, while hazy boundaries are slowly varying from foreground to background. The homogeneousness value

of boundary is lesser than foreground and background. The window size of DXD centered at (x, y) is used for calculating the SD of pixel A (i, j).

$$SD(x, y) = \sqrt{\frac{\sum_{m=x-(D-1)/2}^{x+(D-1)/2} \sum_{n=y-(D-1)/2}^{y+(D-1)/2} (A_{mn} - \mu_{xy})^2}{D^2}} \tag{14}$$

Where μ_{xy} average of intensity is values within window and determined by equation (15).

$$\mu_{xy} = \frac{\sum_{p=x-(D-1)/2}^{x+(D-1)/2} \sum_{q=y-(D-1)/2}^{y+(D-1)/2} A_{pq}}{D^2} \tag{15}$$

The edge values are obtained by discontinuity of pixel A (i, j) which is calculated by Sobel operator.

$$E_g(x, y) = \sqrt{A_x^2 + A_y^2} \tag{16}$$

Where A_x corresponds to horizontal derivative and A_y corresponds to vertical derivative. Now, homogeneity characteristic can be defined by equation (17).

$$HO(x, y) = 1 - \frac{SD(x, y)}{SD_{max} E_{gmax}} \tag{17}$$

Where $SD_{max} = \max \{SD(x, y)\}$ and $E_{gmax} = \max \{E_g(x, y)\}$. The Edge subset ES (x, y) is represented as

$$ES(x, y) = 1 - HO(x, y) \tag{18}$$

The value of ES (x, y) has a range of 0 to 1

Step 5: Method to compute value of α

- (i) (a) mini = smallest {largest values of every column in Edge Subset (ES) ≠ 0}
- (b) α will take any number which is any value less than or equal to mini.
- (ii) NS of image is converted to binary i.e.

The NS of image is converted to binary. O (x, y) is binary form of OS (x, y), E (x, y) is binary form of ES (x, y) and B (x, y) is binary form NOS (x, y) and these are obtained by equation (19), (20) and (21) respectively.

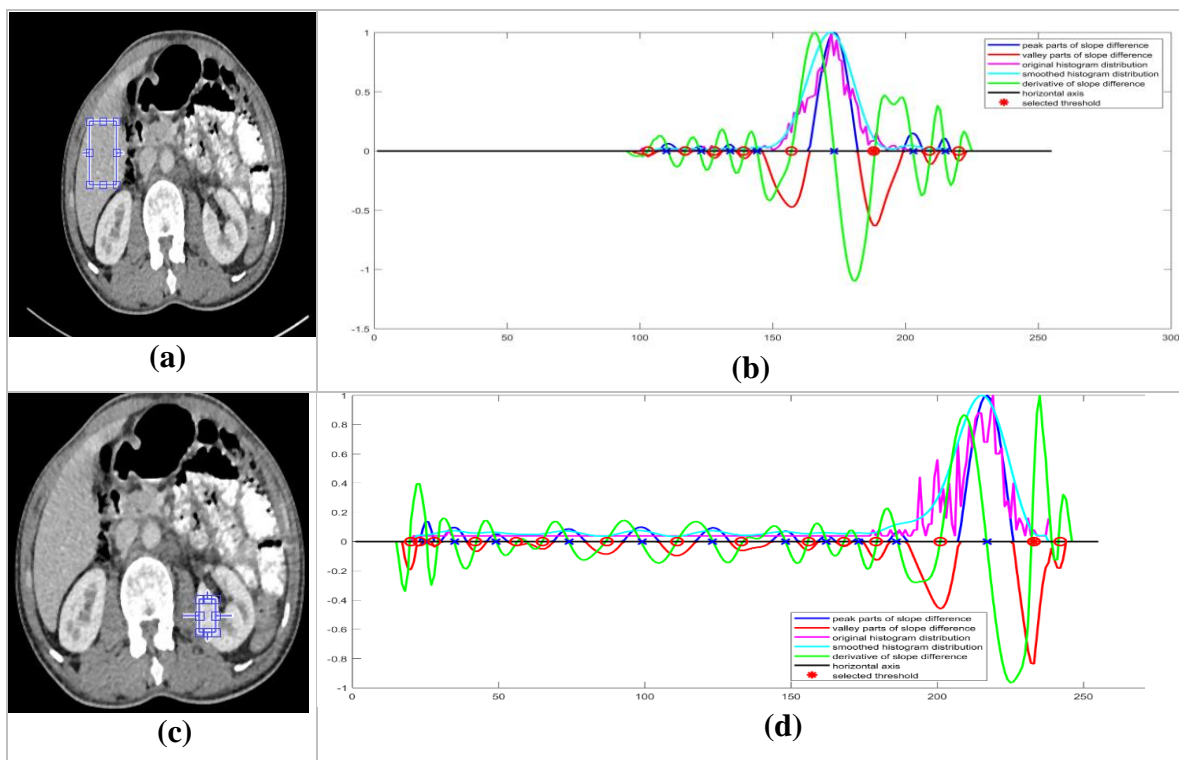
$$O(x, y) = \begin{cases} 1 & OS(x, y) \geq OS_{th}, ES(x, y) < \alpha \quad \square \quad \square \quad \square \quad \square \\ 0 & \text{others} \quad \square \end{cases} \tag{19}$$

$$E(x, y) = \begin{cases} 1 & OS(x, y) < OS_{th} \vee NOS < NOS_{th}, ES(x, y) \geq \alpha \quad \square \quad \square \\ 0 & \text{others} \quad \square \end{cases} \tag{20}$$

$$B(x, y) = \begin{cases} 1 & NOS(x, y) \geq NOS_{th}, ES(x, y) < \alpha \quad \square \\ 0 & \text{others} \quad \square \end{cases} \tag{21}$$

Figure 3: Demonstration of Slope Variation Scatter (SVS); (a) Cropping random section of liver; (b) SVS of liver image; (c) Cropping arbitrary section of kidney image; (d) SVS of kidney image.

Perform morphological operation on edge image to achieve exact output. The framework of proposed model which is combined endeavour of SVS and NS theory to separate intended object from CT scan images is shown in figure 3.



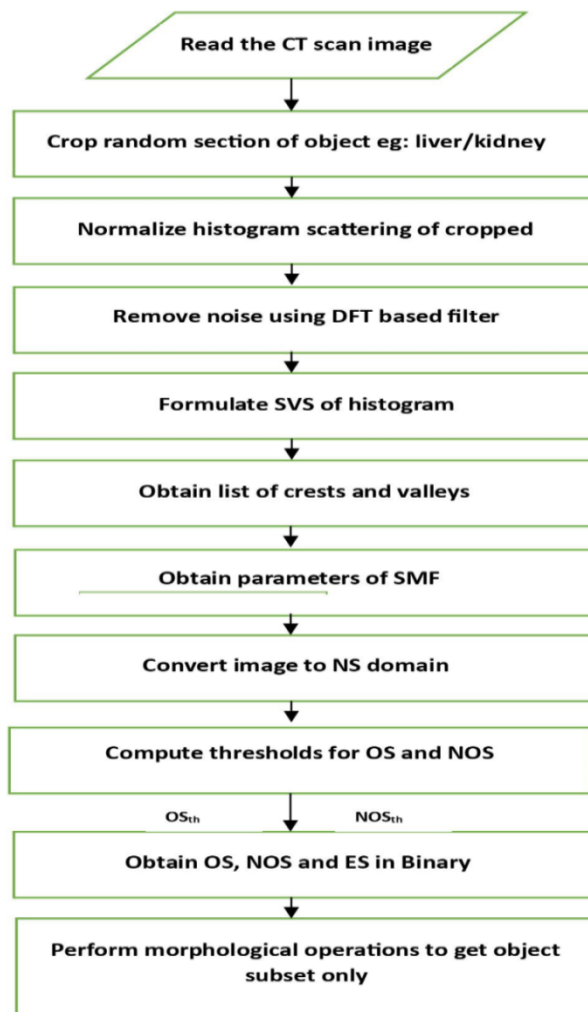


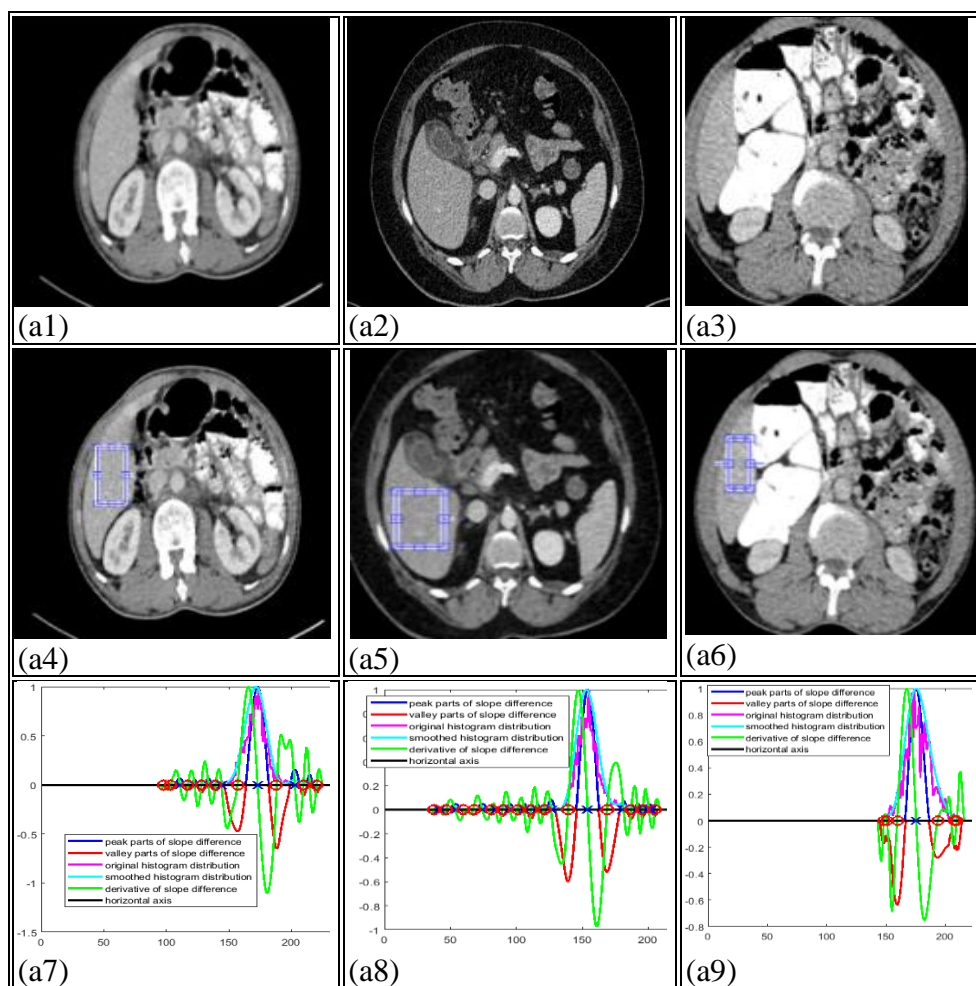
Figure 3: Framework of proposed model

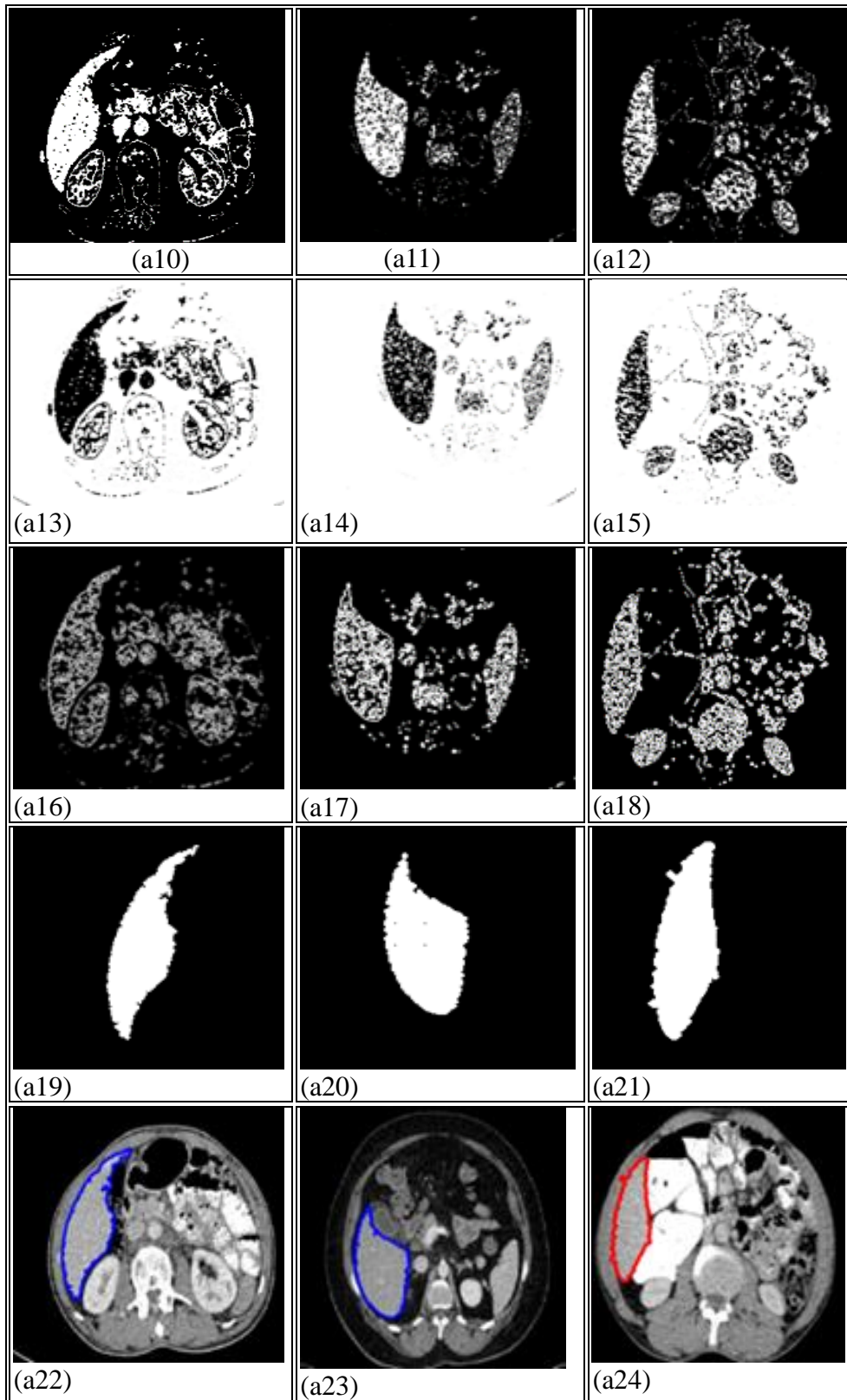
4. Experimental Results

The database for trial and testing contains 106 patients CT scan images collected from M/s Hubli scan centre, Karnataka, India. The images are in colour format of size 1019 x 682. Figure 2 illustrates SVS of randomly cropped liver and kidney image from which NGF parameters are decided. Figure 2(a) and (b) illustrate cropping liver and kidney image from CT scan respectively. Figure (b) and (d) describe SVS plot of liver and kidney respectively. In figure 2(b) and (d), x-axis represents pixel value from 0 to 255; y axis represents normalized pixel density, lilac describes original histogram; whereas sky-blue represents smoothed histogram; Persian Blue exemplifies SVS, the Persian Blue cross corresponds to crest values, red circles on x-axis represents valley value; green indications derivation of SVS.

Figure 4 illustrates experimental results on CT scan to segment the liver. Figure 4(a1),(a2) and (a3) represent CT scan images, 4(a4),(a5) and (a6) demonstrate cropping arbitrary section of liver, 4(a7),(a8) and (a9) show SVS of object image; 4(a10),(a11) and (a12) show OS of image; 4(a13),(a14) and (a15) illustrate NOS of image; 4(a16),(a17) and (a18) show ES of image; 4(a19),(a20) and (a21) represent segmented liver image from abdominal CT scan; 4(a22),(a23) and (a24) show outline marking to liver in CT scan image; 4(a25),(a26) and (a27) show segmentation results of FCM.

Figure 5 illustrates experimental results on CT scan to segment the kidney. Figure 5(b1),(b2) and (b3) represent CT scan images, 5(b4),(b5) and (b6) demonstrate cropping arbitrary section of kidney, 5(b7),(b8) and (b9) show SVS of object image; 5(b10),(b11) and (b12) show OS of image; 5(b13),(b14) and (b15) illustrate NOS of image; 5(b16),(b17) and (b18) show ES of image; 5(b19),(b20) and (b21) represent segmented kidney image from abdominal CT scan; 5(b22),(b23) and (b24) show outline marking to kidney in CT scan image; 5(b25),(b26) and (b27) show segmentation results of FCM.





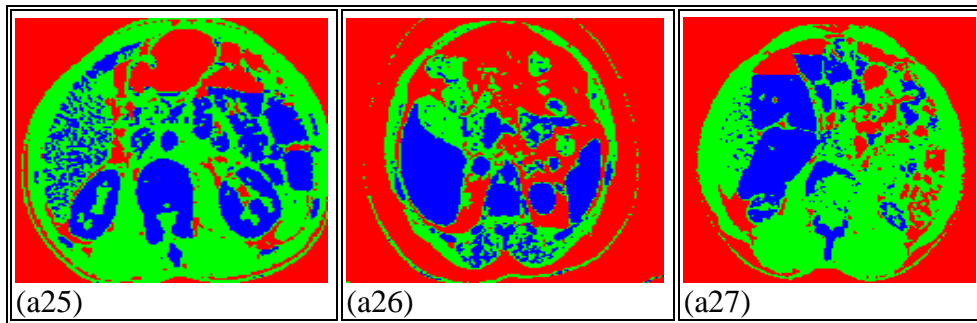
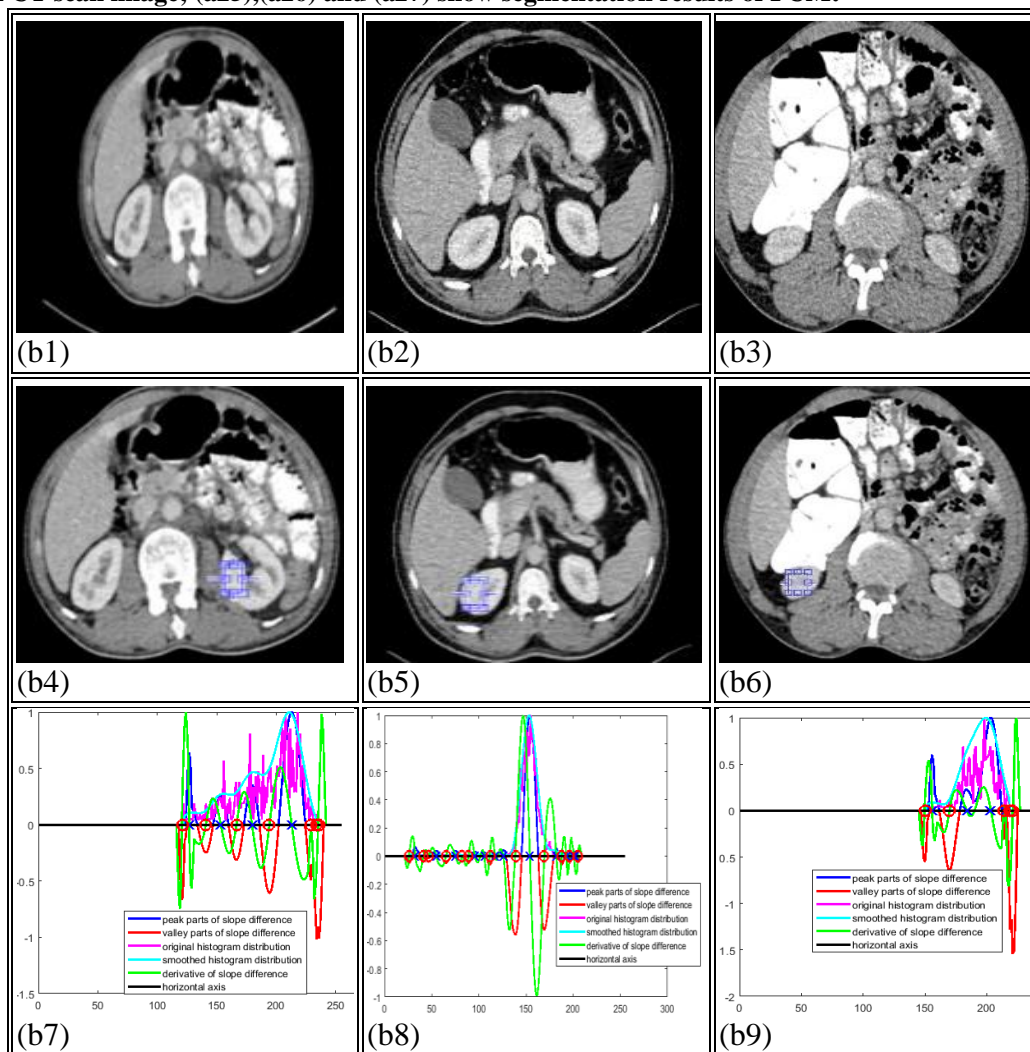
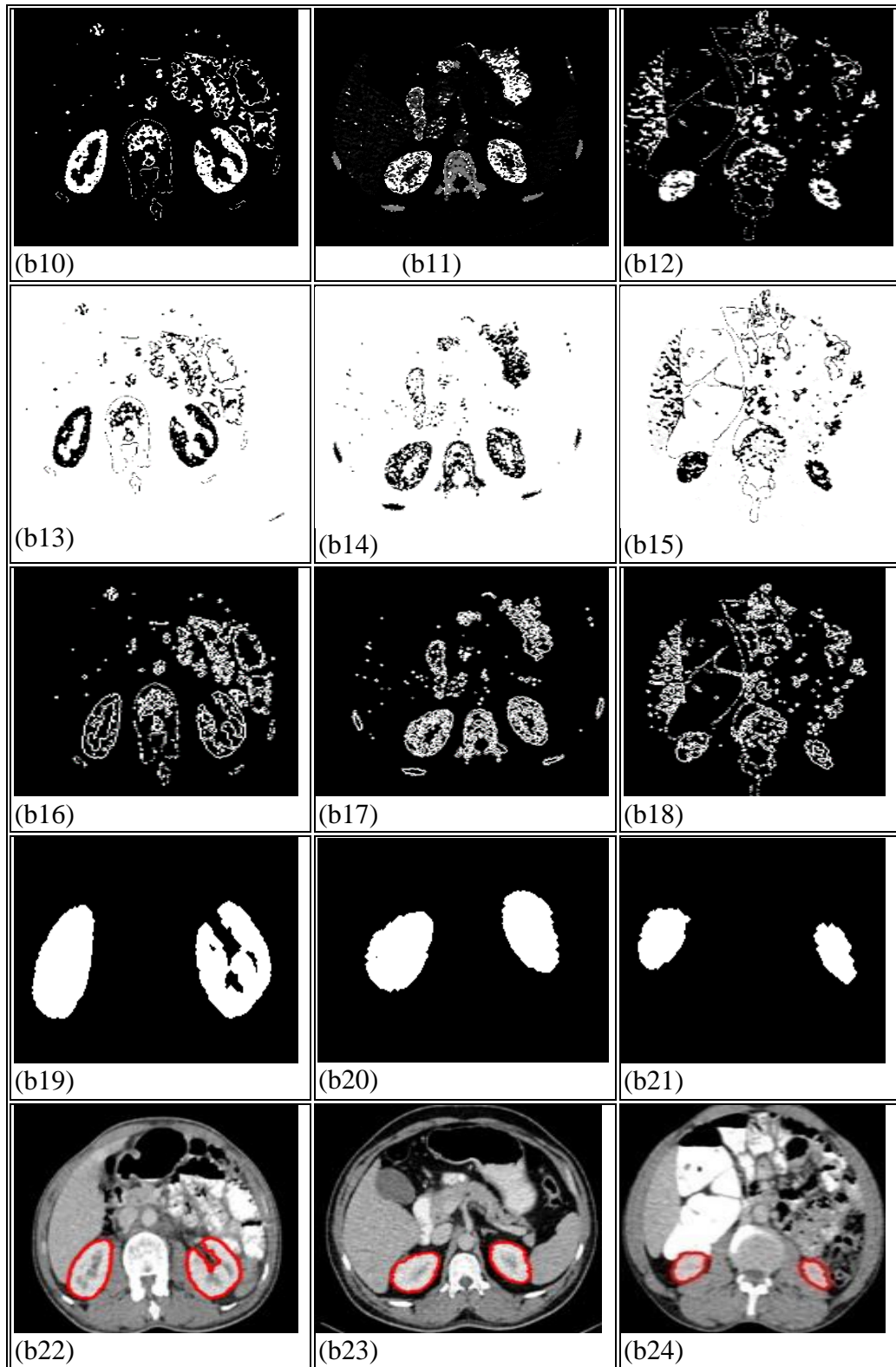


Figure 4: Experimental results of proposed framework for liver segmentation from abdominal CT scan (a1),(a2) and (a3) represent CT scan images, (a4),(a5) and (a6) demonstrate cropping arbitrary section of liver, (a7),(a8) and (a9) show SVS of object image; (a10),(a11) and (a12) show OS of image; (a13),(a14) and (a15) illustrate NOS of image; (a16),(a17) and (a18) show ES of image; (a19),(a20) and (a21) represent segmented liver image from abdominal CT scan; (a22),(a23) and (a24) show outline marking to liver in CT scan image; (a25),(a26) and (a27) show segmentation results of FCM.





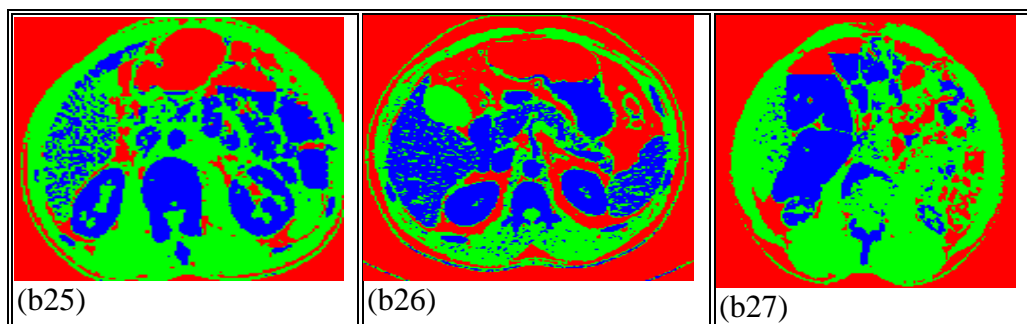


Figure 5: Experimental results of proposed framework for kidney segmentation from abdominal CT scan (b1),(b2) and (b3) represent CT scan images, (b4),(b5) and (b6) demonstrate cropping arbitrary section of kidney, (b7),(b8) and (b9) show SVS of object image; (b10),(b11) and (b12) show OS of image; (b13),(b14) and (b15) illustrate NOS of image; (b16),(b17) and (b18) show ES of image; (b19),(b20) and (b21) represent segmented kidney image from abdominal CT scan; (b22),(b23) and (b24) show outline marking to kidney in CT scan image; (b25),(b26) and (b27) show segmentation results of FCM.

5.Quantitative analysis

The segmentation model with high efficiency and minimal bias are key objectives in surgical planning which will directly impact the results. Hence quantitative estimation of image segmentation model is crucial.

5.1 Accuracy (Acc)

Segmentation accuracy analyses the deviation between annotated image and segmentation predicted image. In this paper, annotated image is approved with the manual segmentation image under supervision of medical practitioner [43]. The similarity between an annotated image and algorithm predicted image reflects the accuracy (Acc). The accuracy measure is calculated as shown in Eq. (22) [48]. The accuracy for liver and kidney for proposed model and FCM is shown in figure 6 and 7 respectively. Acc will be *one* if segmentation is perfect. As Acc moves away from *one* denotes deviation of segmentation.

$$Acc = \frac{\text{correctly classified pixels}}{\text{Total number of pixels}} * 100 \tag{22}$$

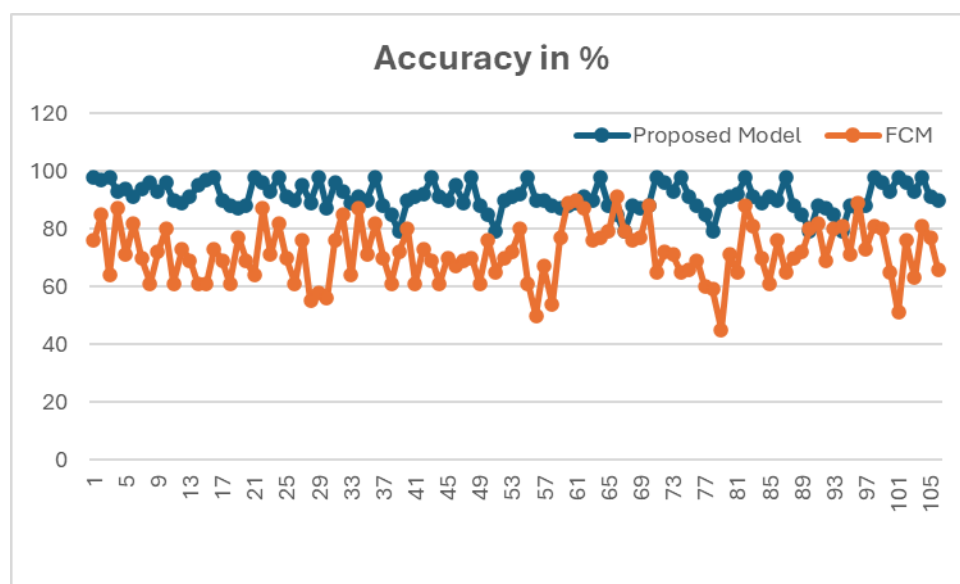


Figure 6: Evaluation of proposed framework and FCM for liver segmentation using Acc.

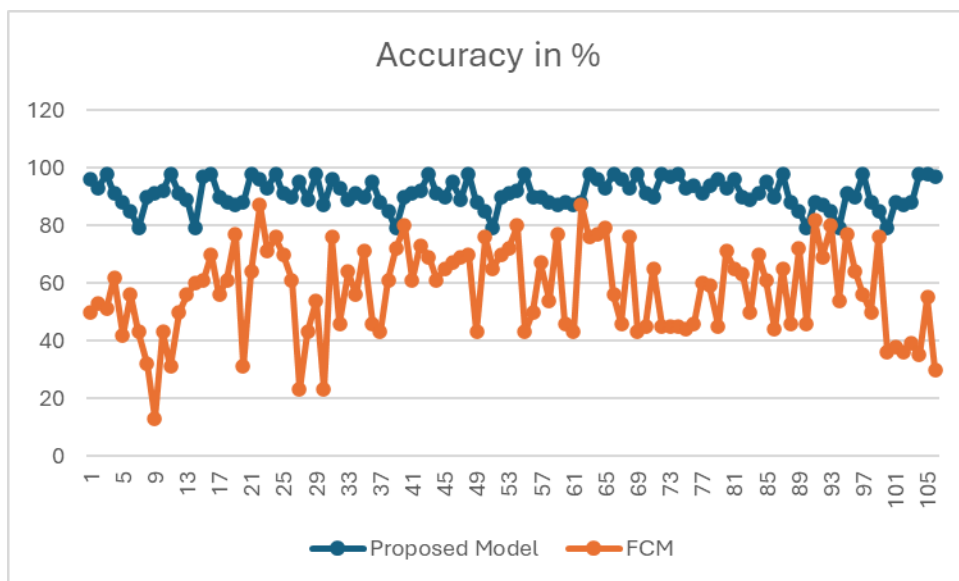


Figure 7: Evaluation of proposed framework and FCM for kidney segmentation using Acc.

5.2 Relative Volume Disagreement (RVD)

The specific RVD exists between 2 images SEG_{ALG} and SEG_{GT} is given in per cent and defined as.

$$RVD = 100 * (|SEG_{ALG} - SEG_{GT}|) / SEG_{GT} \tag{23}$$

with SEG_{ALG} as image segmented by proposed algorithm and SEG_{GT} as ground truth image [37]. A score of 0% indicates that the two areas completely overlap. A comparison of the suggested model with FCM algorithm using RVD for liver and kidney is shown in figure 8 and 9 respectively.

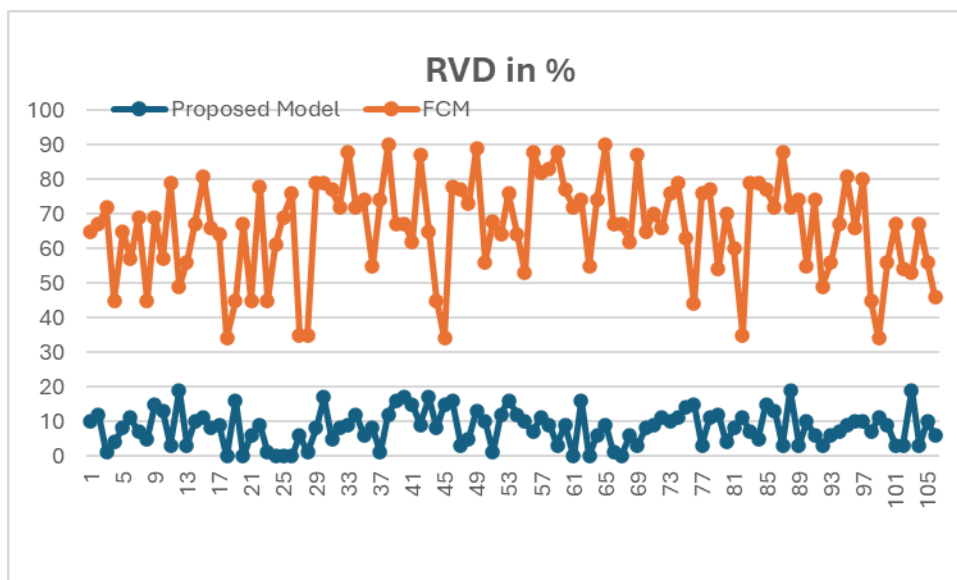


Figure 8: Evaluation of proposed framework and FCM for liver segmentation using RVD.

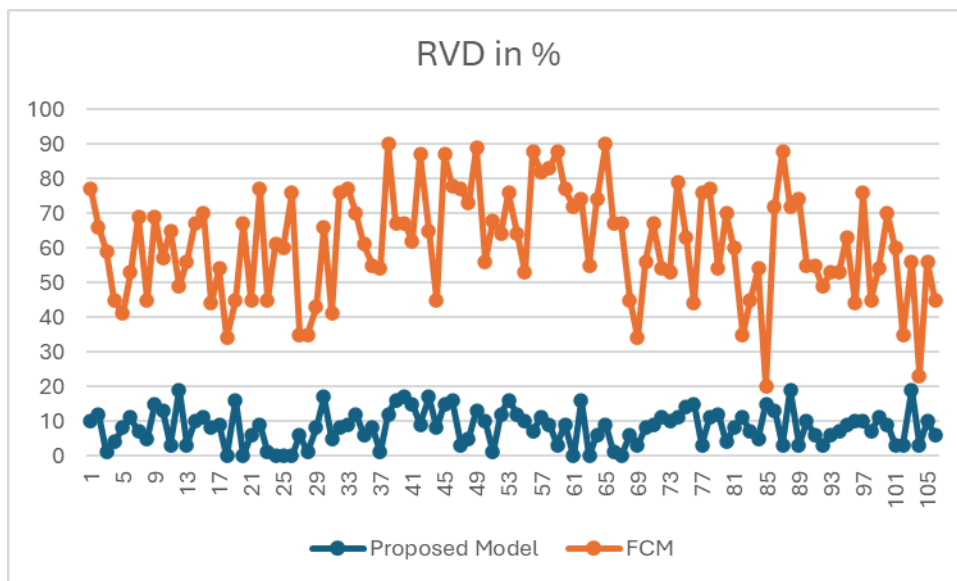


Figure 9: Evaluation of proposed framework and FCM for kidney segmentation using RVD.

5.3 Dice Similarity Factor (DSF)

The similarity of two objects is also evaluated by DSF. In this evaluation technique, Dice’s coefficient needs to be calculated to evaluate similarities [47]. DSF is defined as

$$DSF = 2 * [SEG_{ALG} \cap SEG_{GT}] / [SEG_{ALG} + SEG_{GT}] * 100 \tag{24}$$

where SEG_{ALG} and SEG_{GT} are the segmented and ground truth, respectively. The DSF values are in the 0–100% range. When the value is near 0%, it represents less or no similarity between the segmented and ground truth regions. If the DSF value is near 100%, then the segmented and ground truth regions are more similar. The DSF for liver and kidney for proposed model and FCM is shown in figure 10 and 11 respectively. The tabulation of average accuracy, RVD and DSF for liver and kidney is shown in table 1.

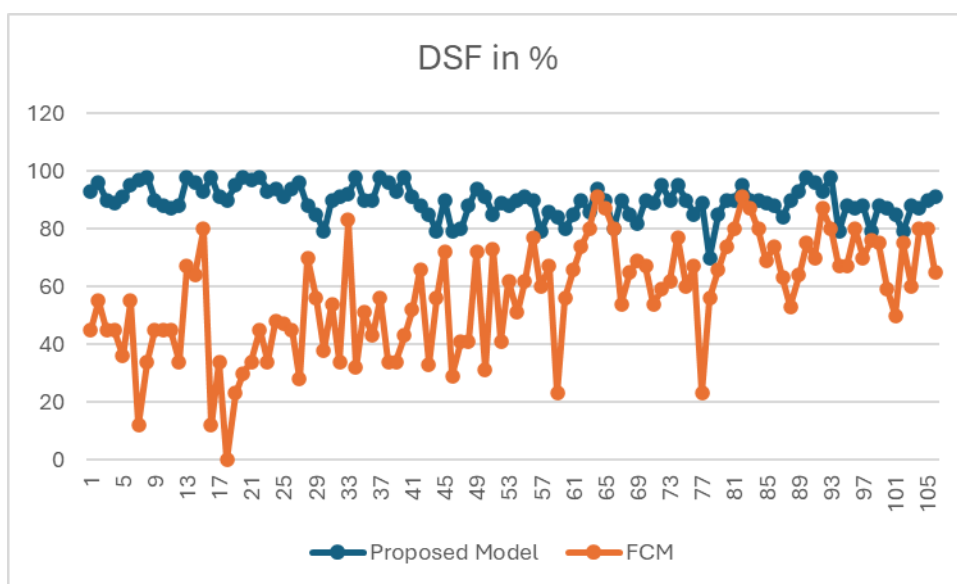


Figure 10: Evaluation of proposed framework and FCM for liver segmentation using DSF.

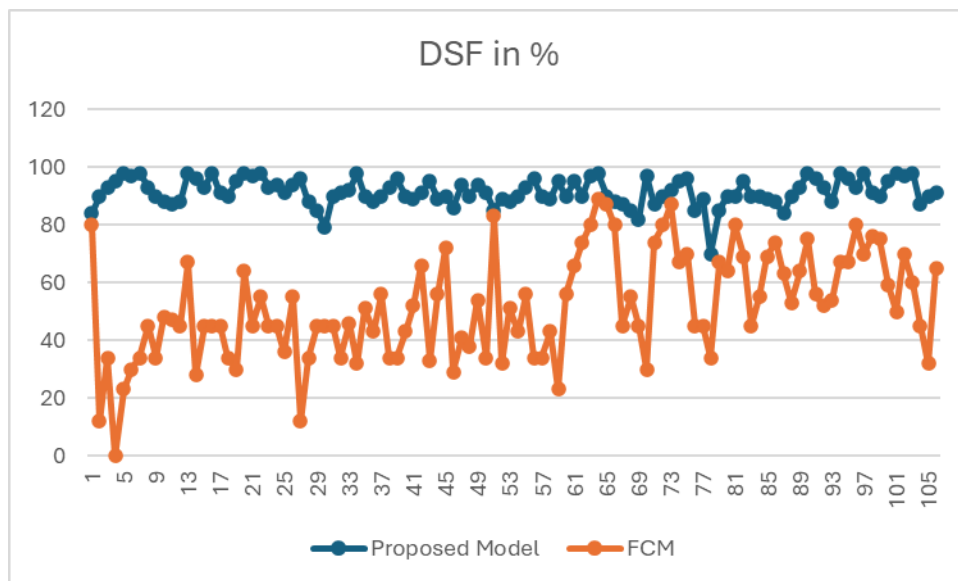


Figure 11: Evaluation of proposed framework and FCM for kidney segmentation using DSF

Table 1: Comparison of average accuracy, RVD and DSF for liver and kidney of proposed model and FCM

Evaluation Metric	Acc	RVD	DSF
Proposed Model			
Liver	91.01%	8.23	89.61
Kidney	91.11%	5.96	91.45
FCM			
Liver	71.58	66	57.02
Kidney	57.13	61.11	52.02

Conclusions

In this paper, the combined endeavour of two mathematical tools is used to obtain the accurate biomedical object segmentation. The first mathematical tool is Slope Variation Scatter plot of intensity variation of object image is obtained. The crests in the SVS provide mean pixel values in the objects. Using Crests present in the SVS, a novel NGF is proposed which converts medical image to NS domain. The NS is a dreadful mathematical tool that illustrates degree of truth, false and indefinity that must be considered as independent event in real time. The proposed model is experimented to separate liver and kidney from the CT scan image accurately. It is observed that results using anticipated framework is far better than Fuzzy-C-Means algorithm.

References

[1] S. Broumi, Bipolar Neutrosophic Minimum Spanning Tree, Smart Application and Data Analysis for Smart Cities, 201–206, 2018. doi: 10.2139/ssrn.3127519.
 [2] Jha S, Kumar R, Priyadarshini I, Smarandache F, Long HV. Neutrosophic image segmentation with dice coefficients. Measurement. 2019 Feb 1;134:762-72.
 [3] Zhao J, Wang X, Li M. A novel Neutrosophic image segmentation based on improved fuzzy C-means algorithm (NIS-IFCM). International Journal of Pattern Recognition and Artificial Intelligence. 2020 May 26;34(05):2055011.

-
- [4] Zhao J, Wang X, Li M. A novel Neutrosophic image segmentation based on improved fuzzy C-means algorithm (NIS-IFCM). *International Journal of Pattern Recognition and Artificial Intelligence*. 2020 May 26;34(05):2055011.
- [5] H. D. Cheng et al., Color image segmentation: Advances and prospects, *Patt. Recogn.* 34(12) (2001) 2259–2281.
- [6] W. Chunyan et al., High resolution remote sensing image segmentation based on the interval type-2 fuzzy model, *Chin. J. Sci. Instr.* 37(3) (2016) 658–666.
- [7] M. Cucuringu et al., Detection of core - periphery structure in networks using spectral methods and geodesic paths, *Eur. J. Appl. Math.* 27(6) (2016) 846–887.
- [8] J. Zhao et al., Side scan sonar image segmentation based on neutrosophic set and quantum-behaved particle swarm optimization algorithm, *Marine Geophys. Res.* 37(3) (2016) 229–241.
- [9] X. Wu et al., Study on industrial automation with SCARA robot vision system design, *Adv. Mater. Res.* 675 (2013) 72–76.
- [10] Luo D, Zhang Y, Li J. Research on Several Key Problems of Medical Image Segmentation and Virtual Surgery. *Contrast Media & Molecular Imaging*. 2022 Apr 11;2022.
- [11] Deheyab AO, Alwan MH, Rezzaqe IK, Mahmood OA, Hammadi YI, Kareem AN, Ibrahim M. An Overview of Challenges In Medical Image Processing. In *Proceedings of the 6th International Conference on Future Networks & Distributed Systems 2022 Dec 15* (pp. 511-516).
- [12] Weese J, Lorenz C. Four challenges in medical image analysis from an industrial perspective. *Medical image analysis*. 2016 Oct 1;33:44-9.
- [13] Oliveira, R. B., Marranghello, N., Pereira, A. S., & Tavares, J. M. R. “A computational approach for detecting pigmented skin lesions in macroscopic images”. *Expert Systems with Applications*, vol.61, pp.53-63, 2016.
- [14] Broumi S, Nagarajan D, Bakali A, Talea M, Smarandache F, Lathamaheswari M, Kavikumar J. Implementation of neutrosophic function memberships using MATLAB program. *Infinite Study*. 2019.
- [15] Smarandache, F., 2019. Neutrosophic set is a generalization of intuitionistic fuzzy set, inconsistent intuitionistic fuzzy set (picture fuzzy set, ternary fuzzy set), pythagorean fuzzy set, spherical fuzzy set, and q-rung orthopair fuzzy set, while neutrosophication is a generalization of regret theory, grey system theory, and three-ways decision (revisited). *Journal of new theory*, (29), pp.1-31.
- [16] Das S, Roy BK, Kar MB, Kar S, Pamučar D. Neutrosophic fuzzy set and its application in decision making. *Journal of Ambient Intelligence and Humanized Computing*. 2020 Nov;11:5017-29.
- [17] Norouzi A, Rahim MS, Altameem A, Saba T, Rad AE, Rehman A, Uddin M. Medical image segmentation methods, algorithms, and applications. *IETE Technical Review*. 2014 May 4;31(3):199-213.
- [18] Panimalar, A., Aarthi, D., Kumar, S.S. *et al.* Analysing Medical Image with Discrete Wavelet Transform Under Uncertainty. *Int. J. Appl. Comput. Math* 9, 114 (2023). <https://doi.org/10.1007/s40819-023-01566-8>
- [19] Thanikachalam V, Kavitha MG, Sivamurugan V. Diabetic Retinopathy Diagnosis Using Interval Neutrosophic Segmentation with Deep Learning Model. *Computer Systems Science & Engineering*. 2023 Mar 1;44(3).
- [20] Talouki AG, Koochari A, Edalatpanah SA. Image completion based on segmentation using neutrosophic sets. *Expert Systems with Applications*. 2024 Mar 15;238:121769.
-

-
- [21] Datta S, Chaki N, Modak B. A novel technique for dental radiographic image segmentation based on neutrosophic logic. *Decision Analytics Journal*. 2023 Jun 1;7:100223.
- [22] Wang Z, Chen Y, Yin J. Application of Improved U-Net with Feature Fusion and Expectation-Maximization Attention in Kidney Tumor Segmentation of CT Images. In *Proceedings of the 2024 4th International Conference on Bioinformatics and Intelligent Computing 2024* Jan 26 (pp. 113-118)..
- [23] Siri, Sangeeta K. and Latte, Mrityunjaya V.. "A Novel Approach to Extract Exact Liver Image Boundary from Abdominal CT Scan using Neutrosophic Set and Fast Marching Method" *Journal of Intelligent Systems*, vol. 28, no. 4, 2019, pp. 517-532. <https://doi.org/10.1515/jisys-2017-0144>
- [24] Siri SK, Latte MV. Combined endeavor of Neutrosophic Set and Chan-Vese model to extract accurate liver image from CT scan. *Computer methods and programs in biomedicine*. 2017 Nov 1;151:101-9.
- [25] Siri SK, Kumar S P, V. Latte M. An improved expectation-maximization algorithm to detect liver image boundary in ct scan images. *IETE Journal of Research*. 2023 Oct 31;69(10):6846-54.
- [26] Siri SK, Pramod Kumar S, Latte MV. Accurate Liver Border Identification Model in CT Scan Images. *International Journal of Image and Graphics*. 2021 Jul 30;21(03):2150039.
- [27] Wang Z. A new approach for segmentation and quantification of cells or nanoparticles. *IEEE Transactions on Industrial Informatics*. 2016 Mar 14;12(3):962-71.
- [28] Wang Z, Yang Y. A non-iterative clustering based soft segmentation approach for a class of fuzzy images. *Applied Soft Computing*. 2018 Sep 1;70:988-99.
- [29] Wang Z. Recognition of occluded objects by slope difference distribution features. *Applied Soft Computing*. 2022 May 1;120:108622.
- [30] Sangeeta K. Siri, S. Pramod Kumar & Mrityunjaya V Latte (2022) Threshold-Based New Segmentation Model to Separate the Liver from CT Scan Images, *IETE Journal of Research*, 68:6, 4468-4475, DOI: [10.1080/03772063.2020.1795938](https://doi.org/10.1080/03772063.2020.1795938).
- [31] Nayantara, P.V., Kamath, S., Kadavigere, R. et al. Automatic Liver Segmentation from Multiphase CT Using Modified SegNet and ASPP Module. *SN COMPUT. SCI*. 5, 377 (2024). <https://doi.org/10.1007/s42979-024-02719-2>.
- [32] Zhang, Z., Li, G., Wang, Z. et al. Deep-learning segmentation to select liver parenchyma for categorizing hepatic steatosis on multinational chest CT. *Sci Rep* 14, 11987 (2024). <https://doi.org/10.1038/s41598-024-62887-2>.
- [33] Leube J, Horn M, Hartrampf PE, Buck AK, Lassmann M, Tran-Gia J. PSMA-PET improves deep learning-based automated CT kidney segmentation. *Zeitschrift Für Medizinische Physik*. 2024 May 1;34(2):231-41.
- [34] Cao G, Sun Z, Wang C, Geng H, Fu H, Yin Z, Pan M. RASNet: Renal automatic segmentation using an improved U-Net with multi-scale perception and attention unit. *Pattern Recognition*. 2024 Jun 1;150:110336.
- [35] Raut PK, Behera SP, Broumi S, Baral A. Evaluation of Shortest Path by using Breadth-First Algorithm under Neutrosophic Environment. *HyperSoft Set Methods in Engineering*. 2024 Jan 17;1:34-45.
- [36] Saini RK, Ahirwar A, Smarandache F, Kushwaha M. Multi-Criteria Group Decision-Making with ELECTRE-III Method for Selection of Female Spouse in Pythagorean Neutrosophic Environment. *Plithogenic Logic and Computation*. 2024 Jan 25;1:36-53.
-

-
- [37] Concepción IP, Almendariz KA, Valdiviezo WV. Neutrosophic Evaluation of Health Promotion Programs for Resource Allocation. *Neutrosophic Optimization and Intelligent Systems*. 2024 Jan 28;1:57-66.
- [38] Srinivasan S, Durairaju K, Deeba K, Mathivanan SK, Karthikeyan P, Shah MA. Multimodal Biomedical Image Segmentation using Multi-Dimensional U-Convolutional Neural Network. *BMC Medical Imaging*. 2024 Feb 8;24(1):38.
- [39] El-Shahat D, Talal N, Ye J, Cui WH. CT Image Segmentation Using Optimization Techniques under Neutrosophic Domain. *Neutrosophic Systems with Applications*. 2024 Apr 1;16:1-1.
- [40] Mostafa NN, Kumar AK, Ali Y. A Comparative Study on X-Ray image Enhancement Based on Neutrosophic Set. *Sustainable Machine Intelligence Journal*. 2024 Apr 21;7:2-1.
- [41] Wang Z, Monitoring of GMAW weld pool from the reflected laser lines for real times control, *IEEE Trans. Ind.* 10(4), (2014) 2073-2083
- [42] Smarandache F. A Unifying Field in Logics: Neutrosophic Logic. *Neutrosophy, Neutrosophic Set, Neutrosophic Probability: Neutrosophic Logic. Neutrosophy, Neutrosophic Set, Neutrosophic Probability. Infinite Study*; 2005.
- [43] Abdel-Basset, M., Smarandache, F. & Ye, J. Special issue on “Applications of neutrosophic theory in decision making-recent advances and future trends”. *Complex Intell. Syst.* 5, 363–364 (2019). <https://doi.org/10.1007/s40747-019-00127-1>
- [44] AboElHamd E, Shamma HM, Saleh M, El-Khodary I. Neutrosophic logic theory and applications. *Neutrosophic sets and systems*. 2021 Mar 31;41:30-51.
- [45] C. Graaf, A. Koster, K. Vincken, and M. Viergever, “Validation of the interleaved pyramid for the segmentation of 3D vector images, ” *Pattern Recognition Letters*, vol. 15, no. 5, pp. 467–475, 1994.
- [46] Elmasry WH, Moftah HM, El-Bendary N, Hassanien AE. Performance evaluation of computed tomography liver image segmentation approaches. In 2012 12th International Conference on Hybrid Intelligent Systems (HIS) 2012 Dec 4 (pp. 109-114). IEEE.
- [47] Jaesik Min, Mark Powell, Kevin W. Bowyer, —Automated Performance Evaluation of Range Image Segmentation Algorithms, *IEEE Transactions on Systems, Man, and Cybernetics—Part B: Cybernetics*, vol. 34, no. 1, February 2004, pp-263-271.
- [48] Kumar SP, Latte MV. Fully automated segmentation of lung parenchyma using break and repair strategy. *Journal of Intelligent Systems*. 2019 Apr 24;28(2):275-89.

Received: April 20, 2024. Accepted: Aug 22, 2024